Chinese Chemical Letters 33 (2022) 2143–2146

Contents lists available at ScienceDirect

Chinese Chemical Letters

journal homepage: www.elsevier.com/locate/cclet

A hybrid organic-inorganic perovskite with robust SHG switching

Mengjuan Yang, Hao Cheng, Yuqiu Xu, Mengzhen Li, Yong Ai*

Ordered Matter Science Research Center, Nanchang University, Nanchang 330031, China

ARTICLE INFO

Article history:
Received 28 July 2021
Revised 18 August 2021
Accepted 22 August 2021
Available online 26 August 2021

Keywords:
Lead hybrid perovskite
Second harmonic generation
Single-crystal X-ray diffraction
Nonlinear optical switching
Halogen substitution

ABSTRACT

Owing to the diversity of structure and potential applications in the field of electrics, sensors, and light-emitting diodes, lead halide perovskites have attracted great attention in recent years. Especially those lead halide perovskites with non-centrosymmetric crystal structures usually exhibit nonlinear optical (NLO) characteristics, which may endow them photoelectricity switching functionality. In this work, a lead-based hybrid organic-inorganic perovskite (HOIP) material, trimethyliodomethylammonium lead trichloride (TMIM·$PbCl_3$), is obtained on the basis of tetramethylammonium lead chloride through halogen substitution on the cation part. It shows dual-phase-transition behavior around 345 and 358 K, which is significantly improved. TMIM·$PbCl_3$ crystallizes in the chiral space group, $P2_12_12_1$, and shows a well-defined second harmonic generation (SHG) response, and good switching endurance, which makes it an excellent candidate for SHG switching material. This work highlights the importance of halogen substitution for crystal engineering and may pave way for the further exploration of the optoelectronic devices.

The perovskite with typical ABX_3 structures (A and B represent two different metal ions, and X represents an anion), especially hybrid organic-inorganic perovskites (HOIPs), have attracted widespread attention in the field of photoelectric devices due to their special optical and electric properties [1–6]. Lead halide HOIPs (*e.g.*, $MAPbI_3$) have been the most intensively investigated optoelectronic materials with their excellent advantages of tunable bandgap, facile synthesis method, and high absorption coeficient [7,8]. However, the increasingly serious concerns of environment toxicity force researchers to explore the future environment friendly lead-free perovskites [9–11]. Nevertheless, the lead halide HOIPs are sometimes the prior options for the research of switchable optoelectronic materials, sensors, solar cells, *etc.* because their properties can be tuned by external stimuli such as temperature, light, and electric [12–15]. The HOIPs who crystallize in one of the 18 non-centrosymmetric point groups are second harmonic generation (SHG) active [16,17]. For example, $(DFCHA)_2PbI_4$, and $(4,4\text{-}DFHHA)_2PbI_4$ which crystallized in space group $Cmc2_1$ and $P2_1$, respectively, exhibited strong SHG response [18,19]. Materials for which the SHG signal could be switched between different states reversibly under external stimulation have been widely investigated for the application in the fields of photo-switching, electro-optical modulators [20–23]. For instance, $[NH_3(CH_2)_5NH_3]SbCl_5$ and NH_2-MIL-53(Al) have been reported with a well-defined SHG switching property [24,25].

Solid state materials with phase transition provide opportunities and possibilities to explore novel SHG switch materials based on structural phase transition with symmetry breaking [26,27]. Reducing the symmetry of the crystals is an efficient way to obtain the non-centrosymmetric structures for crystal designing [28]. The organic cationic part in the HOIP molecules is of great interest thanks to their particular nature that can be favorable to design the polar structure. Chemically modifying the organic moieties of the crystal could lead to the generation of the polarity. It was reported that, for many typical globular shape molecules like tetramethylammonium, quinine and DABCO (1,4-diazabicyclo[2,2,2]octane), the halogen substitution could induce to crystalize in lower symmetry space group and enhance the phase transition point [29,30]. By precise molecular modifications on such molecules, polar crystals and high phase transition temperature materials could be obtained. For example, polar crystals of (TMXM) $FeBr_3$ (X = F, Cl, Br, I) could be acquired through halogen substitution on the cation of the parent crystal (TM)$FeBr_3$ (TM, tetramethylammonium) [31]. Again, halogen substitution leads to the non-centrosymmetric structures of (TMXM)MnX_3 (X = Cl, Br) [32], and (TMCM)CdX_3 (X = Cl, Br) [33,34]. In addition, halogen substitution can effectively increase the phase transition point. Such as $(TMXM)_2PtCl_6$ (X = F, Cl, Br, I) [35].

Inspired by those works in designing polar crystal materials, we hereby report a lead-based 1D chain HOIP trimethyliodomethylammonium lead trichloride (TMIM·$PbCl_3$). Thanks to the

* Corresponding author.
E-mail address: yong.ai@ncu.edu.cn (Y. Ai).

https://doi.org/10.1016/j.cclet.2021.08.098
1001-8417/

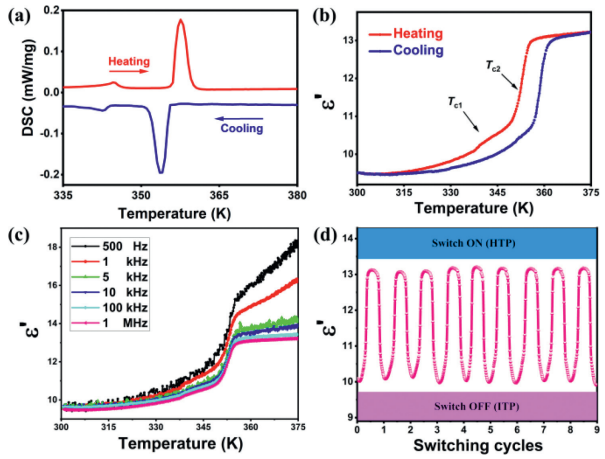

Fig. 1. (a) DSC curves acquired in a heating-cooling cycle of TMIM·$PbCl_3$. (b) Temperature-dependence of the real part (ε') of the dielectric constant of TMIM·$PbCl_3$ at 1 MHz in heating-cooling run. (c) The dielectric constant (ε') of TMIM·$PbCl_3$ under different frequencies from 500 Hz to 1 MHz in heating run. (d) The switching cycles of the dielectric measurement for the TMIM·$PbCl_3$.

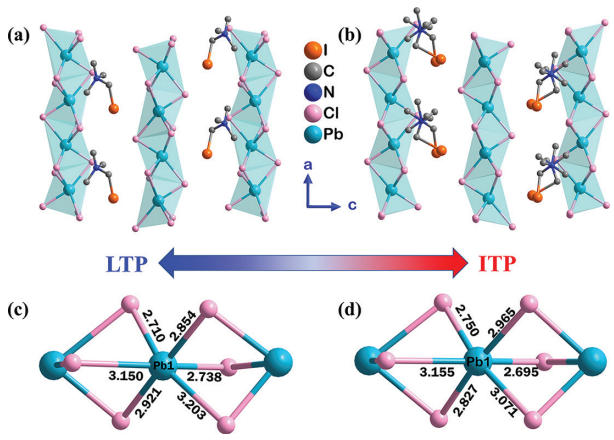

Fig. 2. (a) Packing structures of TMIM·$PbCl_3$ from *b*-axis in 293 K (LTP) and (b) 348 K (ITP), showing the similarities of the crystal structures and the differences of ordered states of the organic TMIM cations. The dashed lines stand for the Cl···I edge interactions. (c) Distorted $PbCl_6$ octahedron with inhomogeneous Pb–Cl bond lengths in 293 K and (d) in 348 K. H atoms were omitted for clarity.

halogen-halogen interaction, TMIM·$PbCl_3$ crystalizes in a non-centrosymmetric space group, $P2_12_12_1$, and has two solid-state phase transitions at 345 K (T_{c1}) and 358 K (T_{c2}), respectively. Compared with the 225 K and 328 K of $[(CH_3)_4N]_4Pb_3Cl_{10}$ in Xue's work [36], the halogen substitution induces a significant increase in the phase transition temperature. TMIM·$PbCl_3$ shows a strong SHG response that is comparable to potassium dihydrogen phosphate (KDP) at room temperature. The SHG signal vanished immediately at temperature above T_{c2}, which indicates a centrosymmetric feature of TMIM·$PbCl_3$ at its high-temperature phase. Moreover, TMIM·$PbCl_3$ shows good switching endurance, with switching contrast of ~2500, which makes it an excellent candidate for SHG switching material. This work will broaden the lead halide organic-inorganic hybrid SHG switches family.

The colorless neddle crystals of TMIM·$PbCl_3$ (Fig. S1 in Supporting information) were collected by evaporating the mixed clear solution of the trimethyliodomethylammonium chloride ([TMIM]·Cl) and $PbCl_2$. The phase transition behavior of TMIM·$PbCl_3$ was firstly studied by differential scanning calorimetry (DSC) with the PerkinElmer Diamond DSC instrument. As shown in Fig. 1a, the endothermic peaks during the heating process and corresponding exothermic peaks in the cooling process suggest two reversible temperature-dependent thermal phase transitions. The transition temperatures are deduced as 345 K (T_{c1}) and 358 K (T_{c2}) from the heating peaks. For convenience, we name the phase below 345 K as low-temperature phase (LTP), the phase above 358 K as high-temperature phase (HTP), and the phase between the two as intermediate temperature phase (ITP). According to the formula $\Delta S = \Delta H/T$, the entropy change ΔS of the two endothermic peaks is calculated as 0.46 and 6.79 J mol^{-1} K^{-1}, respectively. The calculated N values are 1.16 (T_{c1}) and 2.24 (T_{c2}) based on the Boltzmann equation $\Delta S = R\ \ln(N)$, where R represents the gas constant and N stands for the possible orientations number. Such large N values reveal that the compound has a reversible transition between ordered and disordered states [37]. Structural changes are usually accompanied by a variation on calorific value during the heating/cooling progress. The endothermic and exothermic behaviors of phase transition materials endow them a wide range of applications in thermal storage devices [38,39]. In order to explore the thermal stability of TMIM·$PbCl_3$, we conducted a thermogravimetric (TGA) analysis [40,41]. The weight percent versus temperature curve indicates that TMIM·$PbCl_3$ can bear the high temperature up to 520 K, which is 160 K higher than T_{c2} (Fig. S2 in Supporting information). The reversible thermal phase transition and thermal stability make it a potential heat storage material.

To further explore the phase transition, we used the Tong hui TH2828A instrument to measure the compound dielectric ε ($\varepsilon = \varepsilon'$-$i$-$\varepsilon''$). Fig. 1b shows the temperature-dependent dielectric constant of the real part of the complex permittivity (ε') at 1 MHz. There are two reversible dielectric anomalies, which matched well with the phase transition temperature in DSC. The step-shaped dielectric anomalies from ITP to HTP indicates the mutation of dielectric constant in a narrow temperature range. Fig. 1c shows the variation dielectric constant under different frequencies from 500 Hz to 1 MHz in heating run. There are obvious dielectric anomalies at low frequencies around T_{c2}, and as the frequency increases, the amplitude of the change gradually decreases, which means that the crystal is sensitive to external frequencies. Since the dielectric properties are related to temperature, the temperature can be used as a control variable to switch the TMIM·$PbCl_3$ between ITP and HTP. To check the dielectric switching endurance, we carried out the switching of the capacitor by controlling the temperature around T_{c2}. Fig. 1d shows the dielectric constant of TMIM·$PbCl_3$ at 1 MHz under the heating-cooling cycles. The higher dielectric constant region with a temperature above 358 K (HTP) was defined as 'Switch ON', and the area between 346 and 358 K (ITP) as 'Switch OFF'. It shows excellent reversibility and endurance. The on/off conversion by receiving and decoding thermal enables its potential applications for sensor devices. In addition, no obvious dielectric decay was observed during the cycles.

High-quality single crystals were selected for the X-ray Diffraction (XRD) measurement. Rigaku Oxford Diffraction was used to collect variable temperature Single-crystal XRD data with Mo$K\alpha$ radiation (λ = 0.71073 Å) at 293 K (LTP), 348 K (ITP), and 383 K (HTP). TMIM·$PbCl_3$ was refined as the non-centrosymmetric space group $P2_12_12_1$ (No. 19) at LTP. It has a typical ABX_3 perovskite structure. The asymmetric unit consists of one TMIM cation, six Cl^- ligands and one Pb^{2+} atom (Fig. S3 in Supporting information). The unit cell parameters are a = 7.7839(6) Å, b = 9.2515(8) Å, c = 16.1914(14) Å, $\alpha = \beta = \gamma = 90°$, and V = 1165.99(17) $Å^3$ (Table S1 in Supporting information). As shown in Fig. 2a, the anionic part $[PbCl_3]^-_n$ has a typical one-dimensional chain structure that grows along the a-axis. TMIM cations are in the ordered state at room temperature and occupy the cavities in between adjacent $[PbCl_3]^-_n$ chains with the face-sharing $PbCl_6$ octahedra structures. At 348 K, it still crystallizes in the $P2_12_12_1$ space group with cell parameters of a = 7.7947(7) Å, b = 9.2974(11) Å, c = 16.1305(17)

Å, and V = 1169.0(2) Å^3, (Table S1). Although the unit cell parameters of TMIM·$PbCl_3$ in LTP and ITP are very similar, there are obvious changes in structure. The organic cations of the mesophase become disordered from LTP to ITP is shown in Fig. S4 (Supporting information). From the point of view of crystal engineering, hydrogen bonding and halogen bonding is vital for crystal growth [33,42,43]. According to the geometric model established by Desiraju, the halogen···halogen interaction $X_1 = X_2$ ($X_1 \neq X_2$) can be divided into two possible types based on the different θ_1 and θ_2 values, where $\theta_1 = C - X_{heavy} \cdots X_{light}$, and $\theta_2 = C - X_{light} \cdots X_{heavy}$. For the type I, $\theta_1 = \theta_2$, while for the type II, $\theta_1 \approx 180°$ and $\theta_2 \approx 90°$ [44]. TMIM·$PbCl_3$ should be treated as the type II with θ_1 and θ_2 values of 153.7°and 75°, respectively (Fig. S5 in Supporting information). The halogen···halogen interaction between the TMIM cations and the $[PbCl_3]^-_n$ chains form the C-I···Cl-Pb bond with a bond length of 3.303(7) Å at room temperature, as shown in Fig. S2. It was reported that the strength of halogen bonds as the halogen varied from F, Cl to Br [30,33]. The I···Cl halogen bond in the crystal of TMIM·$PbCl_3$ is considerably strong for crystal packing. Such halogen bonds cause the inhomogeneous Pb-Cl bond lengths (Figs. 2c and d, Table S2 in Supporting information) and the strong distortion in the octahedra of $PbCl_6$. The octahedral distortion parameter (Δd) was described by the formula as following [45,46]:

$$\Delta d = \frac{1}{6}\sum\left[\frac{d_n - d}{d}\right]^2 \quad (1)$$

Where d_n represents the Pb-Cl bond length, and d represents the average Pb-Cl bond length, the calculated Δd is 4.05 × 10^{-3}, which is much greater than those reported lead halide perovskites, such as $(C_5H_{13}N_2)PbCl_4{\cdot}H_2O$ (Δd = 2.031 × 10^{-3}) [47], (DMEN)$PbBr_4$ (Δd = 1.74 × 10^{-3}), $(C_6H_{13}N_3)PbBr_4$ (Δd = 2.6 × 10^{-3}) [48]. Because of the 'stretching' of the I···Cl halogen bond interaction, the $[PbCl_3]^-_n$ chains are no longer straightforward along *a*-axis. Instead, as shown in Figs. 2a and b, they show a zigzag conformation, which leads TMIM·$PbCl_3$ to crystallize in the chiral space group, $P2_12_12_1$. This phenomenon is very different from the typical one-dimensional transition metal halogen chains formed perovskites, such as TMBM-$MnBr_3$ [32], (3-pyrrolinium)-$CdBr_3$ [49], *R*/*S*-CYHEAPbI$_3$ [50] and $C_4N_2H_{14}PbCl_4$ [51].

We further measured the crystal structures of TMIM·$PbCl_3$ in the HTP, but it failed because of the weak diffraction. Fortunately, the unit cell parameters were obtained and the hexagonal or trigonal crystal system with cell parameters of a = 9.3601(11) Å, b = 9.3601(11) Å, c = 7.8947(11) Å, $\alpha = \beta = 90°$, $\gamma = 120°$ were collected. In order to explore the structure at HTP, variable temperature powder X-ray diffraction (PXRD) was carried out by Rigaku D/MAX 2000 PC X-ray diffractometer. The simulated and the measured PXRD at room temperature matched well with each other, which supports the purity of the TMIM·$PbCl_3$ (Fig. S6 in Supporting information). The PXRD patterns of TMIM·$PbCl_3$ are quite similar in the LTP (*i.e.*, 293 K, 313 K, 333 K), which indicates that the same phase and no phase change occurs. When the temperature rises between T_{c1} and T_{c2} (*i.e.*, 348 K, 353 K), the PXRD pattern changes significantly. As depicted in region B of Fig. 3a, the intensity of the diffraction peak at 19.1° increases. In region D, the two diffraction peaks at 29.2° and 29.34° merge into a new peak at 29.18°. When the temperature goes to HTP (363 K, 383 K), the diffraction peak at 12.54° in area A and the diffraction peak at 22.9° in area C disappear. The absence of peaks under heating indicates that the crystal has undergone a phase transition from a low symmetry phase to a high symmetry phase.

As shown in Fig. 3c, the SHG intensity of TMIM·$PbCl_3$ is comparable with that of the potassium dihydrogen phosphate (KDP) at room temperature. The strong nonlinear optical (NLO) characteristic of TMIM·$PbCl_3$ can be attributed to its chiral nature ($P2_12_12_1$ space group), which is originated from I···Cl halogen···halogen interaction. According to the variable temperature-dependent SHG measurement in Fig. 3b, the SHG signal starts to drop dramatically at 350 K until the background value at 355 K. The transition temperature (T_{c2}) deduced from SHG versus temperature curve matched well with that obtained from DSC and the dielectric measurements. The weakening of the signal from 350 K is due to the cations disorder in the crystal structure under heating. Above 355 K, the vanishing of the SHG signal reveals the centrosymmetric crystal feature of TMIM·$PbCl_3$.

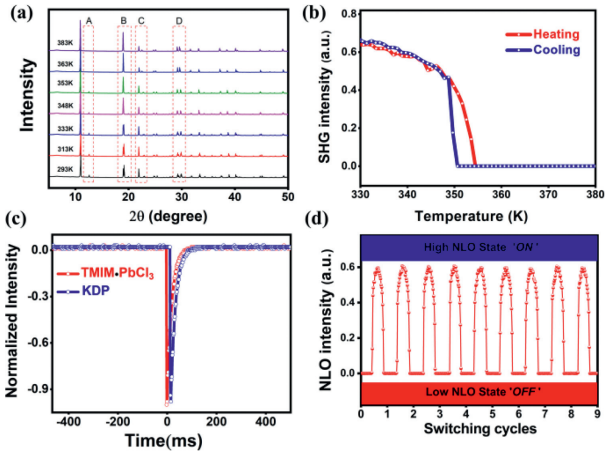

Fig. 3. (a) Variable-temperature PXRD pattern of TMIM·$PbCl_3$ obtained in the temperature range 293–383K. (b) Switchable conversion of SHG signals between high-NLO and low-NLO states. (c) Oscilloscope traces of the SHG signals of TMIM·$PbCl_3$ and KDP at room-temperature. (d) Completely reversible and recoverable switching of NLO effects.

SHG switching property was then investigated. Fig. 3d shows the SHG switching cycles of TMIM·$PbCl_3$. For convenience, we label the high NLO state as 'On' and the low NLO state as 'Off'. The SHG switching maintains the excellent stability. It shows a strong endurance for the fact that it maintains its intensity without significant attenuation during the cycles. Besides, the SHG switcing contrast (the ratio of the on/off intensity) is as large as ~2500, which is higher than those known NLO materials (~150 for single-component plastic crystal [27]; ~40 for organic NLO material [23]; ~38 for metal-organic framework [24]), indicating its good SHG switching performance. The bistable SHG feature of TMIM·$PbCl_3$ makes it an excellent candidate as SHG-switching lead-based perovskites material.

In summary, the ABX_3 type perovskite material TMIM·$PbCl_3$ undergoes two phase transitions around 345 and 358 K. The dual phase transition behavior was carefully investigated by DSC, temperature-dependent dielectric, single-crystal XRD, and variable temperature PXRD. The structural phase transitions are mainly due to the order to disorder change of organic cations under heating. Thanks to the halogen-halogen interaction of C-I···Cl-Pb between the organic cations and anionic $[PbCl_3]^-_n$ chains, TMIM·$PbCl_3$ crystallizes in the non-centrosymmetric space group, $P2_12_12_1$ at room temperature. TMIM·$PbCl_3$ shows a strong SHG signal and robust switching endurance. Therefore, the halogen substitution on globular shape molecules assists the exploration of the lead halide HOIPs type optoelectronic devices.

Declaration of competing interest

The authors declare that they have no known competing financial interests or personal relationships that could have appeared to influence the work reported in this paper.

Acknowledgments

This work was supported by the National Natural Science Foundation of China (No. 21901099).

Supplementary materials

Supplementary material associated with this article can be found, in the online version, at doi:10.1016/j.cclet.2021.08.098.

References

[1] G. Grancini, S. Marras, M. Prato, et al., J. Phys. Chem. Lett. 5 (2014) 3836–3842.
[2] Y.X. Zhao, K. Zhu, Chem. Soc. Rev. 45 (2016) 655–689.
[3] B. Saparov, D.B. Mitzi, Chem. Rev. 116 (2016) 4558–4596.
[4] G. Hodes, Science 342 (2013) 317–318.
[5] S.M. Liu, Y.J. Cao, L. He, et al., Inorg. Chem. 59 (2020) 18396–18401.
[6] Z.X. Wei, Y.H. Zhao, J. Jiang, et al., Chin. Chem. Lett. 31 (2020) 3055–3064.
[7] K. Hong, Q.V. Le, S.Y. Kim, et al., J. Mater. Chem. C 6 (2018) 2189–2209.
[8] Y.X. Zhao, K. Zhu, Chem. Soc. Rev. 45 (2016) 655–689.
[9] G. Schileo, G. Grancini, J. Mater. Chem. C 9 (2021) 67–76.
[10] J. Zhang, X. Gao, Y. Deng, et al., ChemSusChem 8 (2015) 3882–3891.
[11] Y. Li, Z.F. Shi, W.Q. Liang, et al., Mater. Horiz. 8 (2021) 1367–1389.
[12] K. Xu, L. He, Y.Z. Wang, et al., Inorg. Chem. 60 (2021) 10642–10647.
[13] D.Y. Fu, S.C. Wu, J.L. Xin, et al., Chem. Commun. 56 (2020) 14381–14384.
[14] L.J. Zhu, Q.P. Lu, C.H. Li, et al., Chin. Chem. Lett. 32 (2021) 2259–2262.
[15] A. García-Fernández, E.J. Juarez-Perez, J.M. Bermúdez-García, et al., J. Mater. Chem. C 7 (2019) 10008–10018.
[16] W.Q. Liao, J.X. Gao, X.N. Hua, et al., J. Mater. Chem. C 5 (2017) 11873–11878.
[17] P.P. Shi, Q. Ye, Q. Li, et al., Chem. Mater. 26 (2014) 6042–6049.
[18] X.G. Chen, X.J. Song, Z.X. Zhang, et al., J. Am. Chem. Soc. 142 (2020) 10212–10218.
[19] T.T. Sha, Y.A. Xiong, Q. Pan, et al., Adv. Mater. 31 (2019) e1901843.
[20] Y. Yu, M. Nakano, T. Ikeda, Nature 425 (2003) 145 -145.
[21] J.A. Delaire, K. Nakatani, Chem. Rev. 100 (2000) 1817–1846.
[22] B. Champagne, A. Plaquet, J.L. Pozzo, et al., J. Am. Chem. Soc. 134 (2012) 8101–8103.
[23] M.A. Asghar, J. Zhang, S.G. Han, et al., Chin. Chem. Lett. 29 (2018) 285–288.
[24] P. Serra-Crespo, M.A. van der Veen, E. Gobechiya, et al., J. Am. Chem. Soc. 134 (2012) 8314–8317.
[25] G.Q. Mei, H.Y. Zhang, W.Q. Liao, Chem. Commun. 52 (2016) 11135–11138.
[26] Z.H. Sun, J.H Luo, S.Q. Zhang, et al., Adv. Mater. 25 (2013) 4159–4163.
[27] Z.H. Sun, T.L. Chen, X.T. Liu, et al., J. Am. Chem. Soc. 137 (2015) 15660–15663.
[28] P.P. Shi, Y.Y. Tang, P.F. Li, et al., Chem. Soc. Rev. 45 (2016) 3811–3827.
[29] H.Y. Ye, Y.Y. Tang, P.F. Li, et al., Science 361 (2018) 151–155.
[30] X.N. Hua, W.Q. Liao, Y.Y. Tang, et al., J. Am. Chem. Soc. 140 (2018) 12296–12302.
[31] Y. Zhang, X.J. Song, Z.X. Zhang, et al., Matter 2 (2020) 697–710.
[32] W.Q. Liao, Y.Y. Tang, P.F. Li, et al., J. Am. Chem. Soc. 139 (2017) 18071–18077.
[33] W.Q. Liao, Y.Y. Tang, P.F. Li, et al., J. Am. Chem. Soc. 140 (2018) 3975–3980.
[34] Y.M. You, W.Q. Liao, D. Zhao, et al., Science 357 (2017) 306–309.
[35] H. Cheng, M.J. Yang, Y.Q. Xu, et al., ChemPhysChem 22 (2021) 752–756.
[36] C. Xue, S. Wang, W.L. Liu, et al., Chem. Eur. J. 25 (2019) 5280–5287.
[37] J.F. Scott, Science 315 (2007) 954–959.
[38] D.W. Fu, J.X. Gao, W.H. He, et al., Angew. Chem. Int. Ed. 59 (2020) 17477–17481.
[39] K.K. Pillai, B.J. Brinkworth, Appl. Energy 2 (1976) 205–216.
[40] W. Li, Z. Wang, F. Deschler, et al., Nat. Rev. Mater. 2 (2017) 16099.
[41] H.Y. Ye, W.Q. Liao, Q. Zhou, et al., Nat. Commun. 8 (2017) 14551.
[42] A. Mukherjee, S. Tothadi, G.R. Desiraju, Acc. Chem. Res. 47 (2014) 2514–2524.
[43] Z.Z. Wang, X.H. Lv, Y.L. Liu, et al., Inorg. Chem. Front. 4 (2017) 1330–1336.
[44] S. Tothadi, S. Joseph, G.R. Desiraju, Cryst. Growth Des. 13 (2013) 3242–3254.
[45] J.A. Alonso, M.J. Martínez-Lope, M.T. Casais, et al., Inorg. Chem. 39 (2000) 917–923.
[46] M.W. Lufaso, P.M. Woodward, Acta. Crystallogr. B 60 (2004) 10–20.
[47] N. Aizawa, Y.J. Pu, M. Watanabe, et al., Nat. Commun. 5 (2014) 5756.
[48] L. Mao, Y. Wu, C.C. Stoumpos, et al., J. Am. Chem. Soc. 139 (2017) 5210–5215.
[49] P.F. Li, W.Q. Liao, Y.Y. Tang, et al., J. Am. Chem. Soc. 139 (2017) 8752–8757.
[50] Y. Hu, F. Florio, Z. Chen, et al., Science 6 (2020) eaay4213.
[51] G. Wu, C. Zhou, W. Ming, et al., ACS. Energy Lett. 3 (2018) 1443–1449.